Doppler effects in resonant x-ray Raman scattering

Faris Gel'mukhanov,* Hans Ågren, and Paweł Sałek
Institute of Physics and Measurement Technology, Linköping University, S-581 83 Linköping, Sweden
(Received 24 November 1997)

Theory for Doppler effects in resonant x-ray Raman scattering (RXS) is presented. It is shown that the ''electron'' Doppler effect is important in nonradiative RXS for decay transitions between continuum nuclear states lying above the dissociation threshold, and that the averaging of the RXS cross section over molecular orientations can lead to strong non-Lorentzian broadenings of the atomiclike resonances. The Doppler effect is found to give a unique possibility to distinguish dissociating identical atoms, because different peaks correspond to atoms with opposite Doppler shifts. Spectral features of the atomiclike profile are predicted and analyzed. Strong oscillations of the RXS cross section will occur as a consequence of the interference of the Auger electrons. Due to the Doppler effect and the interference, the atomiclike profile can be associated with supernarrow spectral features, the width of which goes below the lifetime broadening and is practically independent of the spectral distribution of the incident radiation. As another consequence of the oscillations and strong anisotropy caused by the interference, we predict parity selection rules for Auger decay transitions in both bound and dissociative systems. The corresponding experiments can be realized by measurements of resonant Auger of surface adsorbed molecules and for molecules by the electron-ion coincidence technique. [S1050-2947(98)07304-1]

PACS number(s): 33.20.Rm, 33.50.Dq

I. INTRODUCTION

The development of synchrotron instrumentation using tunable narrow-band-pass radiation has made it possible to connect Auger electron and x-ray emission spectroscopies to a number of physical processes or effects in the x-ray wavelength region [1–6]. The high spectral quality has not only rendered the possibility to analyze observed features by electronic structure theory, molecular-orbital theory for free systems and band theory for solids, but also to resolve effects that require an account of the nuclear motion. These include vibrational and phonon coupling for bound states, and the nuclear dynamics in dissociative potentials that makes both atomiclike and molecularlike contributions to the x-ray scattering cross section. With ongoing investments in new instrumentation, there is reason to anticipate further progress in spectral quality and that concepts like ''thermal energy,'' ''rotational motion,'' and ''Doppler shifts'' will become relevant in the analysis of coming experiments.

The purpose of this work is to attempt to forestall some of the anticipated development by presenting a theory of x-ray Raman scattering (RXS) taking account of Doppler effects, and to demonstrate a variety of physical phenomena caused by this effect. The theory is general, covering both radiative and nonradiative x-ray scattering and any character of the states involved, but most emphasis is placed on the situation where the Doppler effects are most conspicuous, namely, for nonradiative (Auger) scattering of molecules core excited above the dissociation threshold. As is well known, the RXS spectrum then consists of two qualitatively different parts, the so-called ''molecularlike'' and ''atomiclike'' parts. According to theory [7] the atomiclike contribution caused by decay transitions in one of the dissociation fragments has a width equal to the lifetime broadening, something confirmed by the experimental investigations of the resonant Auger spectra of HCl [8,9]. We generalize this result here, and show that for large release energies following dissociation and accompanying large electron Doppler effects, the atomic Auger resonance can be strongly non-Lorentzian. The Doppler shift can thus exceed the lifetime broadening for a kinetic-energy release in the region $\epsilon \sim 1-10$ eV, which is not uncommon for dissociating molecules [10,11], but which is substantially larger than the thermal energy $k_B T \simeq 0.03$ eV. In the case of heteroatomic molecules, the electron Doppler shift will be smaller for RXS of the heavy atom because the released kinetic energy is transferred mainly to light atom. A typical example is the HCl molecule investigated in Refs. [8,9], where the chlorine Auger resonance thus shows Lorentzian profiles despite comparatively large release energy. In molecules with comparable atomic masses the electron Doppler shift for the dissociative resonance is sufficiently large to exceed the lifetime broadening several times (for example, $\mathbf{k}\cdot v_A \sim 0.2-0.5$ eV for molecules like O_2 with $\Gamma = 0.09$ eV, where $\mathbf{k}$ is a momentum of the Auger electron).

We investigate the anisotropy of ion yields in the Auger Raman experiment, and predict that strong anisotropy of the ion propagation can be measured in an electron-ion coincidence spectroscopy. The electron Doppler shifts for atoms propagating in opposite directions have opposite signs, and this leads to the possibility of distinguishing atoms in the electron-ion coincidence spectra of homonuclear diatomic molecules. It is found that averaging over molecular orientations leads to Doppler broadening of the atomiclike profile, since the electronic Doppler shift depends on the angle between the Auger electron propagation and the molecular

*Permanent address: Institute of Automation and Electrometry, 630090 Novosibirsk, Russia.

axis. It is furthermore shown that the interference effect is important for the atomiclike profile of symmetrical molecules, adding yet another example in x-ray Raman spectroscopy where channel interference plays a crucial role in systems with identical atoms [12–19]. The reason for this effect can be found in the interference contribution to the x-ray scattering cross section. It leads to spectral features and structural information for both electron-ion coincidence and x-ray Raman spectroscopies. It is shown that under certain circumstances the interference leads to a supernarrow peak or hole in the atomiclike profile, narrower than the function of the exciting photons. We also focus on the role of the interference for selection rules of the resonant Auger process.

The paper is organized as follows. Section II gives some brief facts about Doppler effects in x-ray spectra. It is followed by Sec. III, which gives a phase analysis of the scattering amplitude, and which shows that the origin of the Doppler shift can be found in the site-dependent phase of the scattering amplitude. The approximation of the frozen molecular orientation used in the present paper is substantiated in Sec. III A. In Sec. III B the generalized bound-continuum and continuum-continuum Franck-Condon factors leading to the electron Doppler shift are derived. The electron Doppler shift and the recoil effect are discussed in Sec. III C, while Sec. IV is devoted to an analysis of anisotropical and other spectral features caused by the electron Doppler effect in heteronuclear molecules, and which can be measured in electron-ion coincidence spectroscopy. The averaging procedure for the RXS cross section over molecular orientations and Doppler broadening of the atomiclike profile is described in Sec. V. In the subsequent sections the theory is extended to molecules with identical atoms: The beginning of Sec. VI provides expressions for the direct and interference contributions to the scattering cross section. In Secs. VI A and VI C, we discuss the parity selection rules and the role of the interference in the formation of the molecularlike and atomiclike resonances for the broad class of systems with small electron Doppler effects. The principal possibility to use electron-ion coincidence measurements and to distinguish oppositely propagating identical atoms is shown in Sec. VI B. In Sec. VI C, the cross section for an A_2 molecule is averaged over molecular orientations. In Secs. VI D and VI D 2 we show that the atomiclike profile of molecules with identical atoms consists of the supernarrow peak or hole with the spectral width below both the lifetime broadening and the width of the incident radiation. A strict proof of the exact cancellation of the lifetime broadening in these peaks or holes is given in Appendix B. The qualitative explanation of the machinery for the formation of these supernarrow features is given in Sec. VI D 1. Our findings are discussed and concluded in Sec. VIII.

II. BRIEF ACCOUNT OF DOPPLER EFFECTS IN X-RAY SPECTRA

In the soft-x-ray region the thermal motion of the molecules can give additional broadening. Indeed, the total initial and final energies of the photon plus molecule system for the Auger process are $\omega+\mathcal{E}_0+MV^2/2$ and $(M\mathbf{V}+\mathbf{k}_{\rm ph}-\mathbf{k})^2/2M+E+\mathcal{E}_f$, respectively. Here $\mathbf{V}$ is the velocity of a center of gravity of a molecule with mass M; $\mathbf{u}$ and $\mathbf{k}$ are the photoelectron velocity and momentum of the target molecule in the laboratory frame of reference; $\mathbf{k}_{\rm ph}$ is the incoming photon momentum; and $\mathcal{E}_0$ and $\mathcal{E}_f$ are total internal molecular energies for the ground and final states. In this paper we will use the system of atomic units. According to the energy conservation law the photoelectron energy $E=u^2/2$ has a shift

$$E=\omega-\omega_{f0}-\epsilon'-(\mathbf{k}_{\rm ph}-\mathbf{k})\cdot\mathbf{V} \tag{1}$$

caused by molecular motion, where ϵ' is the kinetic energy released under dissociation of the molecule. The term $\mathbf{k}_{\rm ph}\cdot\mathbf{V}$ is the well-known Doppler shift caused by the photon momentum $\mathbf{p}_{\rm ph}$. This shift is negligibly small in the soft-x-ray region due to the small value of the photon momentum $k_{\rm ph}=\omega/c\simeq\omega/137$ (for example, $k_{\rm ph}\simeq 0.14$ a.u. for O_2). This means that ordinary Doppler broadening often can be neglected in x-ray spectroscopy. One can also anticipate that Doppler effects are difficult to identify in the hard-x-ray region due to large lifetime broadening and poor spectral resolution.

The shift $\mathbf{k}\cdot\mathbf{V}$ in Eq. (1) is analogous to the Doppler shift, but is larger and arises from the combination with the electron momentum $\mathbf{k}$ [20] (for example, $k\simeq 6$ a.u. for O_2). This electron Doppler broadening $\mathcal{D}_T=kV\sqrt{\ln 2}$ depends on the temperature T and on the excitation energy through the thermal velocities $\bar{v}=\sqrt{2k_BT/M}$ and $k=\sqrt{2E}$, respectively. Here k_B is the Boltzmann constant.

To get an idea about the Doppler broadening, one can consider the x-ray resonant photoemission spectra (RPE) of carbon monoxide. The comparison of different broadenings for the C $1s\rightarrow\pi^*$ RPE spectra of the CO molecule ($\mathcal{D}_T\simeq 20$ meV, $\Gamma\simeq 42.5$ meV) [21] shows that the broadening $\mathcal{D}_T$ caused by thermal motion of molecules must be taken into account in the analysis of highly resolved RPE spectra. This example demonstrates the typical case when the electronic Doppler broadening $\mathcal{D}_T$ caused by thermal motion at room temperature ($k_BT\simeq 0.03$ eV) is smaller than the lifetime broadening. Recalling the large kinetic energy (1–10 eV) released under dissociation one can understand that the electron Doppler effect in dissociative states is the largest among the cases mentioned.

III. PHASE ANALYSIS OF SCATTERING AMPLITUDE AND THE DOPPLER EFFECT

For the sake of transparency we consider resonant x-ray scattering by a simple three-level diatomic molecule AB with the reduced mass $\mu=m_Am_B/(m_A+m_B)$ (Fig. 1), and with core excitation of atom A (x-ray scattering by homonuclear diatomic molecules is considered in Sec. VI). As shown below, the Doppler effect in radiative RXS is usually small in comparison with the lifetime broadening Γ, while it is more important in the nonradiative case (Raman Auger). Due to this fact and for the sake of convenience we focus the presentation on resonant Auger scattering, but keep in mind that the material covered in this paper easily can be extended to the radiative RXS case.

The energy ω of x-ray photons with wave vector $\mathbf{k}_{\rm ph}$ and polarization vector $\mathbf{e}$ is passed during the scattering to the Auger electron of energy $E=k^2/2$ and momentum $\mathbf{k}$, and to

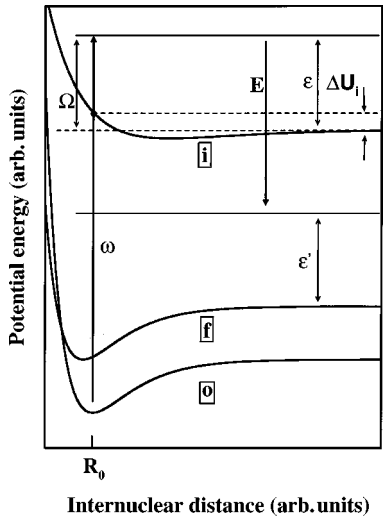

FIG. 1. Scheme of spectral transitions.

the molecule excited from the ground $|O\rangle$ to the final electronic state $|f\rangle$. We take special interest in core excitation above the dissociation threshold of the potential surface $U_i(x)$, thus when specific ''atomiclike'' narrow resonances appear [7,9]. A qualitative picture of the formation of narrow atomiclike resonances with broad short- and long-wave wings [7,9] is given in Fig. 2. Contrary to the wings that follow a Raman-Stokes dispersion law, the energy positions of the atomiclike resonances do not depend on the excitation energy [7–9]. As one can see in Fig. 1, the nuclear states $|\epsilon,i\rangle$ and $|\epsilon',f\rangle$ for the core excited and final electronic states are lying in the continuum having nuclear kinetic energies at infinite separation $\epsilon=p^2/2\mu$ and $\epsilon'=p'^2/2\mu$, respectively. The continuum nuclear wave functions are here normalized to a δ function: $\langle j,\epsilon|\epsilon_1,j\rangle=\delta(\epsilon-\epsilon_1)$. The double differential RXS cross section for a fixed molecular orientation and monochromatic excitation reads [2,14]

$$\sigma(E,\omega)=|F|^2, \quad \epsilon'=\omega-E-\omega_{f0}-(\mathbf{k}_{\rm ph}-\mathbf{k})\cdot\mathbf{V}, \quad (2)$$

where $\omega_{j0}=U_j(\infty)-U_0(R_0)-\omega_0/2(j=i,f)$, R_0 is the ground-state equilibrium interatomic distance, $U_j(x)$ is the interatomic potential of the jth electronic state, and ω_0 is the frequency of the vibrational state $|0\rangle$ of the ground electronic state. For brevity the notation $\sigma(E,\omega)$ is used here instead of $d\sigma(E,\omega)/dE\,dO$. The lifetime broadening of the final state Γ_f is often small in comparison with the lifetime broadening Γ of the core excited states, and in comparison with the spectral width of incident radiation. Therefore, Γ_f is neglected in Eq. (2).

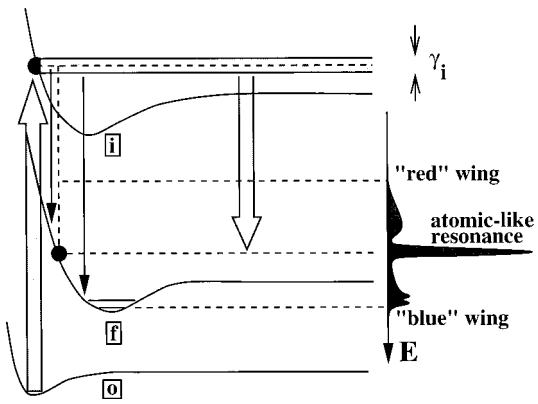

FIG. 2. Formation of the atomiclike resonance with ''blue'' and ''red'' wings.

To start, we investigate the properties of the RXS cross section for the fixed-in-space molecular orientation (2). The physical meaning and applicability of this ''sudden'' approximation will be described in Sec. III A (the procedure of the averaging of this cross section over molecular orientations is also deferred, to Secs. V and VI C). We start from the phase analysis of the resonant part of the scattering amplitude [22,2,14]

$$F\propto\int d\mathbf{R}\Psi^*_{\mathbf{P}'}(\mathbf{R})\Psi_{\mathbf{P}}(\mathbf{R}) \times\int d\epsilon\,\frac{\langle f,\epsilon'|Q_{fi}|\epsilon,i\rangle\langle i,\epsilon|\mathbf{e}\cdot\mathbf{D}_{i0}e^{\imath\mathbf{k}_{\rm ph}\cdot\mathbf{R}_A}|0\rangle}{\Omega-\epsilon-\imath\Gamma}. \quad (3)$$

Here $\mathbf{R}_A$ and $\mathbf{R}$ are the radius vectors of the atom A and the center of gravity of the molecule, respectively, $\mathbf{D}_{i0}$ is the dipole matrix element between core excited and ground electronic states, and $\Omega=\omega-\omega_{i0}$ is the detuning of the incident photon frequency from the resonant frequency ω_{i0} of the adiabatic photoabsorption transition. The wave function $\Psi_{\mathbf{P}}(\mathbf{R})=(2\pi)^{3/2}\exp(\imath\mathbf{P}\cdot\mathbf{R})$ describes the free motion of the center of gravity of the molecule with the momentum $\mathbf{P}=M\mathbf{V}$. In Eq. (3), we have taken into account the condition of completeness for the continuum wave functions $\Psi_{\mathbf{P}}(\mathbf{R})$ in the intermediate core excited state.

The atomiclike decay transition $i\rightarrow f$ in the radiative x-ray Raman scattering is dictated by the dipole selection rules

$$Q_{fi}=\mathbf{e}^*\cdot\mathbf{D}_{fi}e^{-\imath\mathbf{k}'_{\rm ph}\cdot\mathbf{R}_A} \quad (4)$$

with $\mathbf{e}'$ and $\mathbf{k}'_{\rm ph}$ as the polarization vector and momentum of final photon.

In the dissociative region the spectral transition is essentially atomiclike, and all electronic wave functions involved in this decay are very close to those of the atom A. We consider here the case of high-energy Auger electrons, which allows us to express the wave function of this electron, $\psi_{\mathbf{k}}(\mathbf{r})$ relative to the nucleus A,

$$\psi_{\mathbf{k}}(\mathbf{r})=\psi_{\mathbf{k}}(\mathbf{r}-\mathbf{R}_A)e^{\imath\mathbf{k}\cdot\mathbf{R}_A}. \quad (5)$$

This means that the Coulomb matrix element has a phase factor

$$Q_{fi}=Q^A_{fi}e^{-\imath\mathbf{k}\cdot\mathbf{R}_A}, \quad (6)$$

since the Auger transition in the considered case can be assumed to take place in the isolated atom A. The Coulomb matrix element Q^A_{fi} is calculated with $\psi_{\mathbf{k}}(\mathbf{r}-\mathbf{R}_A)$.

A. Molecular rotation and RXS duration

Both the RXS cross section and amplitude were written for the fixed molecular orientation; see Eqs. (2) and (3). The approximation of fixed-in-space or frozen molecular orienta-

tion under scattering [23,3,14] means that the molecule has no time to rotate during the RXS event [24–26],

$$\tau=(\Omega_s^2+\Gamma^2)^{-1/2}. \tag{7}$$

Here $\Omega_s=\omega-\omega_{i0}^s$ denotes the detuning from the resonant frequency of the sudden or vertical photoabsorption transition $\omega_{i0}^s=U_i(R_0)-U_0(R_0)-\omega_0/2$.

The molecular orientation can be considered as frozen if the RXS duration time τ is shorter than the period of molecular rotation τ_r,

$$\tau<\tau_r. \tag{8}$$

One can easily show that this condition is fulfilled for RXS: The effective rotational frequency ω_r has the order of magnitude of the thermal energy k_BT in accordance with the Boltzmann distribution: $k_BT\simeq 0.03$ eV for room temperatures. So the approximation of frozen orientation (8) is valid for molecules and detunings with $(\Omega_s^2+\Gamma^2)^{1/2}>0.03$ eV. One can see that even light molecules like O_2 with $\Gamma=0.09$ eV lack the time to rotate during the RXS process. This analysis may be done also in a stationary representation for the scattering amplitude with strict rotational wave functions $|jm\rangle$ and corresponding vibrational states $|\epsilon,i\rangle$ using the condition of completeness $1=\Sigma_{jm}|jm\rangle\langle jm|$ and the method applied earlier for the vibrational problem [7,24,26].

Due to the emission of a fast Auger electron, the molecule receives a recoil which can accelerate the molecular rotation and hence shorten the rotation rate τ_r up to $1/\delta E_{\rm rot}$. Even for light molecules like O_2 the change of the rotational energy $\delta E_{\rm rot}$ due to the recoil does not exceed 0.06 eV (see Appendix A). However, this recoil energy can be comparable with the width of the supernarrow peaks and holes discussed in Sec. VI D.

B. Generalized Franck-Condon factors

Due to the nuclear motion, the coordinate $\mathbf{R}_A$ of atom A is shifted relative to the equilibrium site $\mathbf{R}_A^0$ by the distance $\delta\mathbf{R}_A$. To calculate the nuclear matrix elements in Eq. (3), we need the expression for $\mathbf{R}_A$ through the normal coordinate $\mathbf{x}=\mathbf{R}_A-\mathbf{R}_B$ of relative motion and through the center of gravity of the molecule $\mathbf{R}=(m_A\mathbf{R}_A+m_B\mathbf{R}_B)/(m_A+m_B)$

$$\mathbf{R}_A=\alpha\mathbf{x}+\mathbf{R},\quad \mathbf{R}_B=-\beta\mathbf{x}+\mathbf{R},$$

$$\alpha=\frac{\mu}{m_A},\quad \beta=\frac{\mu}{m_B}. \tag{9}$$

The Born-Oppenheimer approximation allows one to rewrite the RXS amplitude (3) as follows

$$F\propto a_{\mathbf{n}}\delta(\mathbf{P}'-\mathbf{P}-\mathbf{k}_{\rm ph}+\mathbf{k})\times\int d\epsilon\frac{\langle f,\epsilon'|e^{-\imath\mathbf{k}\cdot\mathbf{x}\alpha}|\epsilon,i\rangle\langle i,\epsilon|e^{\imath\mathbf{k}_{\rm ph}\cdot\mathbf{x}\alpha}|0\rangle}{\Omega-\epsilon-\imath\Gamma}. \tag{10}$$

The amplitude of the resonant x-ray scattering by atom B is also given by this expression if $\exp(-\imath\mathbf{k}\cdot\mathbf{x}\alpha)$ and $\exp(\imath\mathbf{k}_{\rm ph}\cdot\mathbf{x}\alpha)$ are replaced by $\exp(\imath\mathbf{k}\cdot\mathbf{x}\beta)$ and $\exp(-\imath\mathbf{k}_{\rm ph}\cdot\mathbf{x}\beta)$, respectively.

The momentum conservation law $(\mathbf{P}'=\mathbf{P}+\mathbf{k}_{\rm ph}-\mathbf{k})$ describing the photon and electron recoil effects yields immediately the Doppler shift in Eqs. (1) and (2). One recalls here that for the final description of the Doppler effect caused by the thermal motion, the cross section (2) must be convoluted with the Maxwellian distribution $\propto\exp(-MV^2/2k_BT)$. The δ function in Eq. (10) and the small photon and electron Doppler shifts $(\mathbf{k}_{\rm ph}-\mathbf{k})\cdot\mathbf{V}$ will not further be taken into account due to the smallness of the Doppler effect caused by the thermal motion of molecules (see the discussion in Sec. II).

The factor $a_{\mathbf{n}}=\mathbf{e}\cdot\mathbf{D}_{i0}Q_{fi}^A$ depends on the unit vector $\mathbf{n}$ along the molecular axis $(\mathbf{x}=x\mathbf{n})$ through the dipole moment $\mathbf{D}_{i0}$. The dependence of $a_{\mathbf{n}}$ on the internuclear distance x enters mainly via the decay amplitude Q_{fi}^A. This dependence is not so important for the here discussed dissociative or atomiclike resonance which is formed by the spectral transitions in one of the isolated atoms (A). So the decay factor $Q_{fi}^A(x)$ is approximated here by its asymptotical value $Q_{fi}^A\simeq Q_{fi}^A(\infty)$.

Let us evaluate the Franck-Condon (FC) factors connected with the photoabsorption transition assuming the harmonic approximation for the ground-state vibrational wave function $|0\rangle=(\pi a_0^2)^{-1/4}\exp(-[(x-R_0)/a_0]^2/2)$. The effective length scale in this integral is the effective amplitude of vibrations $a_0=(\mu\omega_0)^{-1/2}$, and allows an estimation of $k_{\rm ph}(x-R_0)$ as $k_{\rm ph}a_0$. As a rule this parameter is small (for example, $k_{\rm ph}a_0\sim 10^{-2}\ll 1$ for O_2), and one can replace the exponent $\exp[\imath\alpha\mathbf{k}_{\rm ph}\cdot(\mathbf{x}-\mathbf{R}_0)]$ in the considered FC factor by 1, giving the final result [7]

$$\langle i,\epsilon|e^{\imath\mathbf{k}_{\rm ph}\cdot\mathbf{x}\alpha}|0\rangle=G(p)e^{\imath\alpha\mathbf{k}_{\rm ph}\cdot\mathbf{R}_0}, \tag{11}$$

$$G(p)\equiv\langle i,\epsilon|o\rangle\simeq 2\mu\left(\frac{2\mu b^3}{\pi^{1/2}a_0}\right)^{1/2}\exp\left[-\frac{1}{2}\left(\frac{\Delta\epsilon}{\gamma_i}\right)^2\right]\quad\text{if } b\ll a_0,$$

where $\Delta\epsilon=\epsilon-\Delta U_i$, $\Delta U_i=U_i(R_0)-U_i(\infty)$, $\gamma_i=\mathcal{F}_i a_0$, $b=(2\mu\mathcal{F}_i)^{-1/3}$, and $\mathcal{F}_i=-(dU_i/dx)_0$ is the slope of the interatomic potential $U_i(x)$ for the core excited state at the equilibrium point R_0. This asymptote differs slightly from Eq. (19) in Ref. [7], where $\Delta\epsilon$ contains $-\mathcal{F}_i b$. The term is neglected here in the expression for $\Delta\epsilon$, which also gives better agreement of the asymptote (11) obtained by direct numerical calculations of the bound-continuum FC factor. The phase factor $\exp(\imath\alpha\mathbf{k}_{\rm ph}\cdot\mathbf{R}_0)$ is very important for hard RXS by symmetrical molecules with identical atoms [14], since then the phase multiplier destroys the coherence between the scattering channels through the identical atoms. In the case of radiative RXS this destructive interference leads to the violation of the selection rules for the x-ray scattering tensor [14]. Here we will consider only the case of soft x rays $(k_{\rm ph}R_0\ll 1)$ for which the phase factor $\exp(\imath\alpha\mathbf{k}_{\rm ph}\cdot\mathbf{R}_0)$ can be replaced by unity.

To understand the main spectral and anisotropic features of the RXS amplitude we need to know the generalized continuum-continuum FC factors. Focusing on the continuum-continuum transitions in the dissociative region, we thus need to know the continuum nuclear wave functions

mainly in this region. The dissociating atoms are here moving in a constant potential $U_j(\infty)$ with the plane-wave function

$$|\epsilon,j\rangle=\left(\frac{2\mu}{\pi p}\right)^{1/2}\sin[p(x-x_j)+\varphi_j],$$

$$\varphi_j=\int_{x_j}^{\infty}(p_j-p)dx+\frac{\pi}{4}. \tag{12}$$

Here $j=i,\ f,\ p_j=\{2\mu(\epsilon-[U_j(x)-U(\infty)])\}^{1/2}$, and x_j is the classical turning point where $p_j=0$. We will assume below that $|\epsilon,j\rangle=0$ in the classically inaccessible region $x<x_j$. The exact value of the scattering phase can be found directly from the Schrödinger equation or from the semiclassical formula (12). The classical turning points x_i, x_f as well as the scattering phases φ_i and φ_f for the core excited and final-state potentials depend on the energies ϵ and ϵ', respectively (the energy labels for these quantities are dropped here since we will need the values of x_j and φ_j only for $\epsilon=\Omega$). According to the Condon principle, the value of x_i is close to R_0.

From the continuum wave functions (12), the second generalized FC factor can be evaluated analytically as

$$\begin{aligned}\langle f,\epsilon'|e^{-\imath\mathbf{k}\cdot\mathbf{x}\alpha}|\epsilon,i\rangle=&\frac{\mu}{2(pp')^{1/2}}\,e^{-\imath qx_i}\\&\times\Bigg[e^{\imath\varphi}\delta(p-p'+q)\\&+e^{-\imath\varphi}\delta(p-p'-q)\\&+\frac{1}{\pi}\Bigg\{2\,\sin(\tilde{\varphi})\wp\left(\frac{1}{p'+p}\right)\\&+\imath\Bigg[e^{\imath\varphi}\wp\left(\frac{1}{p'-p-q}\right)\\&-e^{-\imath\varphi}\wp\left(\frac{1}{p'-p+q}\right)\Bigg]\Bigg\}\Bigg],\end{aligned}$$

$$x_i\geqslant x_f, \tag{13}$$

where

$$q=\alpha k\,\cos\,\theta,\quad \varphi=\varphi_f-\varphi_i+p'\Delta,\quad \Delta=|x_i-x_f|, \tag{14}$$

$\tilde{\varphi}=\varphi_i+\varphi_f+p'\Delta$, θ is the angle between the momentum $\mathbf{k}$ of the Auger electron and the molecular axis $\mathbf{x}$, and $\mathcal{P}$ is the principal value. This axis coincides here with the propagation direction of the dissociation fragments. The continuum FC factor for $x_i<x_f$ is again given by Eq. (14) after permutations: $i\rightleftharpoons f$, $p\rightleftharpoons p'$. Here we used the natural assumption of infinitesimal damping of continuum wave functions (12) at infinity ($x\to\infty$). This assumption relates to the fact that atoms at the core excited potential surface have no time to propagate to $x=\infty$ owing to the finite duration [Eq. (7)] of the RXS event.

C. Electron Doppler effect and the recoil energy

The continuum wave function (12) consists of two waves, $\exp(\pm\imath px)$. The momentum exchange of the emitted Auger electron with these two oppositely propagated waves leads to two spectral peculiarities of the FC factor $p=p'\pm q$ [Eq. (13)] caused by a recoil under emission by the atom A of the Auger electron with the momentum $\mathbf{k}$. According to the momentum conservation law, the Auger electron transfers momentum q along the molecular axis to the quasifree atom A. This leads to the change of the relative momentum p. The change of the momentum of atom $A(\alpha k\,\sin\,\theta)$ in the perpendicular direction is not so important for the discussed effect (see Appendix A).

From the physical point of view it is important to consider the energy conservation law

$$\epsilon=\epsilon'\pm\mathbf{v}_A'\cdot\mathbf{k}+\frac{q^2}{2\mu}. \tag{15}$$

The last term in this expression is the electron recoil energy, while the second term is analogous to the photon Doppler effect for the moving atom A with the velocity $\mathbf{v}_A'=\mathbf{n}\alpha p'/\mu$. However, contrary to the photon Doppler effect, the vector $\mathbf{k}$ is the momentum of the Auger electron. So this effect can be coined the ''electron Doppler effect'' (see Sec. II).

IV. ANOMALOUS ANISOTROPY OF AUGER ELECTRON AND ION YIELDS

To succeed in the evaluation of the scattering amplitude (10), we take into account only resonance contributions in Eq. (13). In this resonant approximation one thus neglects the nonresonant term $\wp[1/(p+p')]$, and continue the integration over p up to $-\infty$. We also assume that the energy and momentum released under dissociation are sufficiently large: $p\simeq p'\simeq p_0\gg\eta$, where $p_0=\sqrt{2\mu\Omega}$ and $\eta=\Gamma\sqrt{\mu/2\Omega}$. This condition is equivalent to $\Omega\gg\Gamma$.

An estimation for O_2 shows that the following three parameters are small: $\eta/p_0=\Gamma/2\Omega\sim\Gamma/2\Delta U_i\sim10^{-2}$ (with $\Delta U_i\sim2$ eV), $q/p_0\sim10^{-1}$, and $qp/\mu\gamma_i\sim10^{-1}$. Since we aim to investigate the spectral shape of the atomiclike resonance, the parameter $|p'-p_0|/p_0\sim|E-\omega_{if}|/\Delta U_i$ is also assumed to be small. Finally, expression (10) for the scattering through the core excited state in atom A becomes

$$F=f\times\begin{cases}e^{-\imath qx_i}, & \varphi=\varphi_f-\varphi_i+p_0\Delta \quad \text{if } x_i\geqslant x_f\\ e^{-\imath qx_f}, & \varphi=\varphi_i-\varphi_f+p_0\Delta \quad \text{if } x_f>x_i,\end{cases} \tag{16}$$

with

$$f\propto a_n\times\begin{cases}\dfrac{e^{\imath\varphi}G(p_0)}{\nu+kv_A'\,\cos\,\theta-\imath\Gamma}+\dfrac{e^{-\imath\varphi}\{G(p')-G(p_0)\}}{\nu-kv_A'\,\cos\,\theta-\imath\Gamma} & \text{if } x_i\geqslant x_f\\ G(p_0)e^{-\Gamma\Delta/v_0}\,\dfrac{e^{\imath\varphi}}{\nu+kv_A'\,\cos\,\theta-\imath\Gamma} & \text{if } x_f>x_i,\end{cases} \tag{17}$$

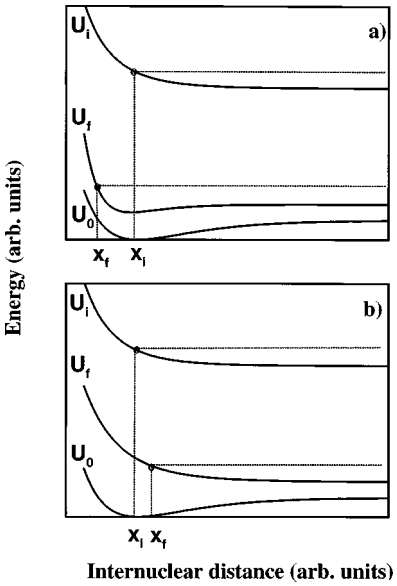

FIG. 3. Positions with different significance of the classical turning point for the final potential surface.

and $\nu = E - \omega_{if}$. The electron Doppler shift $kv'_A \cos\theta$ depends on the velocity $v'_A = \alpha p'/\mu$ of the atom A after emission of the Auger electron. Here $p' = (2\mu[\Omega - (E - \omega_{if})])^{1/2}$, $v_0 = (2\Omega/\mu)^{1/2}$ is the relative atomic velocity corresponding to the kinetic energy $\epsilon = \Omega$. In the latter expression for f, only the main contribution is retained.

One can see that the scattering amplitude is suppressed by $\exp(-\Gamma t)$ times if the final state turning point x_f is further away than x_i. The reason of this quenching is the following. Due to the photoabsorption, the nuclear wave packet is created in the core excited potential surface close to the turning point x_i. The Auger decay channel responsible for the formation of the atomiclike resonance ($\epsilon' = \Omega$) is strongly suppressed during the propagation time $t = \Delta/v_0$ of this wave packet, since the decay transitions to the final states with the same energy $\epsilon' \simeq \Omega$ would occur in the classically inaccessible region (see Fig. 3). During this delay t the population of the core excited state and hence the RXS amplitude decreases by $\exp(-t\Gamma)$. The site-dependent electronic phase factor $\imath q x_f$ [Eq. (16)] is defined by the turning point x_f (the Auger transitions responsible for the formation of the atomiclike resonance becomes allowed from this point). When $x_f < x_i$ the Auger decay with $\epsilon' \simeq \Omega$ starts right away after photoabsorption without delay. In this case the site-dependent phase is equal to $\imath q x_i$. We will see in Sec. VI that both these untrivial facts, that is, the lifetime damping of the RXS amplitude and the phase shift, play crucial roles in the formation of the atomiclike profile of diatomic homonuclear molecules.

Resonant cone of dissociation

At this stage we explore the main contribution to the RXS cross section (2),

$$\frac{1}{(E - \omega_{if} + kv'_A \cos\theta)^2 + \Gamma^2}. \tag{18}$$

This expression concerns electron-ion coincident spectroscopies with the experimental fixation of the molecular axis (via a direction of dissociation) and the direction of the Auger electron propagation.

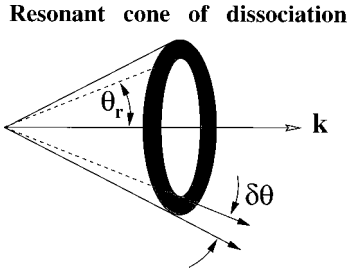

FIG. 4. Resonant cone of dissociation.

Experimental investigations [27–29] have clearly shown the anisotropy of dissociation in the angle-resolved photoelectron-photoion spectroscopy. This anisotropy, hidden in the anisotropy factor $a_{\mathbf{n}}$, is smoother in comparison with the strongly resonant ion yield (18) caused by the Doppler effect. The latter equation shows that the electron-ion coincidence signal changes drastically if the Auger electron energy E lies in the Doppler band $-kv'_A < E - \omega_{if} < kv'_A$. When the lifetime broadening Γ is smaller than the electron Doppler shift kv'_A, the photoions or the fragment of dissociation propagate in the narrow angular interval

$$\delta\theta \simeq \frac{\Gamma}{kv'_A} \tag{19}$$

close to the cone surface (Fig. 4) $\theta \simeq \theta_r$:

$$\cos\theta_r = \frac{\omega_{if} - E}{kv'_A} \quad \text{if} \quad \left|\frac{\omega_{if} - E}{kv'_A}\right| \leqslant 1. \tag{20}$$

The appearance of the narrow *resonant cone of dissociation* with ''resonant'' angle θ_r is one of the important results of the studied problem. Equation (19) clearly demonstrates the strong correlation between propagation directions of the Auger electron and the ion A^+.

V. AVERAGING OF THE CROSS SECTION OVER MOLECULAR ORIENTATIONS

We consider now the spectral shape of atomic-like resonances in the Auger spectrum of atom A in molecule AB with different atoms (the principally different case of identical atoms is treated in Sec. VI C). In this case the cross section emanates entirely from the scattering amplitude for atom A (to be specific, only the case $x_i > x_f$ will be considered in this section). For ordinary resonant Auger measurements of gas-phase molecules, the cross section must be averaged over molecular orientations. We know that two qualitatively different physical reasons are responsible for the dependence of the scattering amplitude (16) on the molecular orientation. As shown in Sec. IV, the first reason is the Doppler effect which leads to a sharper resonant dependence of the cross section on the molecular orientation (18). The second reason is the orientation of the molecular axis **n** relative to the polarization vector **e** and the Auger electron momentum **k**. This smooth polynomial dependence is hidden in the factor $a_{\mathbf{n}}$. This allows to extract the factor $|a_{\mathbf{n}^0}|^2$ from

the integral over the molecular orientation at the resonant angle (20), leading to the following additional averaging of this factor over all $\mathbf{n}^0$ of the cone. Using this averaging together with Eqs. (2) and (16), one obtains

$$\overline{\sigma}(E,\omega)=\sigma_0\Bigg[\rho\{G^2(p_0)+[G(p')-G(p_0)]^2\} + \frac{\Gamma}{E-\omega_{if}}\chi\cos(2\varphi)G(p_0)[G(p')-G(p_0)]\Bigg]. \tag{21}$$

All unessential quantities are collected in $\sigma_0 \propto\langle|a_{\mathbf{n}^0}|^2\rangle 2\pi/\Gamma$. The spectral shape of the cross section is defined by the two functions

$$\rho=\frac{1}{2\pi k v'_A}\left[\arctan\left(\frac{E-\omega_{if}+kv'_A}{\Gamma}\right) - \arctan\left(\frac{E-\omega_{if}-kv'_A}{\Gamma}\right)\right],$$
$$\chi=\frac{1}{2\pi k v'_A}\ln\left(\frac{(E-\omega_{if}+kv'_A)^2+\Gamma^2}{(E-\omega_{if}-kv'_A)^2+\Gamma^2}\right). \tag{22}$$

The Doppler shift

$$kv'_A\cos\theta=k\alpha\left[\frac{2}{\mu}[\Omega-(E-\omega_{if})]\right]^{1/2}\cos\theta \tag{23}$$

depends on the Auger electron energy E (see Fig. 6). The energy dependence of the electron wave number $k=\sqrt{2E}$ can be neglected when E is large.

To understand the main spectral features of the RXS cross section, let us for a while neglect the E dependence of kv'_A. The ρ function is in this case a symmetrical function relative to the resonance $E-\omega_{if}=0$ normalized to unity: $\int dE\ \rho=1$. The integral of χ is equal to zero ($\int dE\ \chi=0$) since χ is an antisymmetrical function relative to the resonant energy $E=\omega_{if}$. The asymptotes of the ρ function

$$\rho=\begin{cases}\dfrac{1}{2kv'_A}\Theta\left(\dfrac{E-\omega_{if}}{kv'_A}\right) & \text{if } \Gamma\ll kv'_A \\ \dfrac{\Gamma}{\pi[(E-\omega_{if})^2+\Gamma^2]} & \text{if } \Gamma\gg kv'_A\end{cases} \tag{24}$$

show directly the crucial role of the electron Doppler effect and of the chaotical molecular orientation on the formation of the atomiclike spectral profile. Here $\Theta(x)$ is the rectangular function: $\Theta(x)=1$ if $|x|\leqslant 1$ and $\Theta(x)=0$ if $|x|>1$. The shape of this dissociative resonance is close to a Lorentzian only if the Doppler shift is small [7], $kv'_A\ll\Gamma$.

When kv'_A exceeds Γ, the position of the atomiclike resonance (18)

$$E=\omega_{if}-kv'_A\cos\theta \tag{25}$$

strongly depends on the molecular orientation via the Doppler shift $kv'_A\cos\theta$. This leads to a broadening of the RXS spectral profile in the dissociative region since the total atomiclike resonance is the sum of the partial atomiclike resonances (18) over all molecular orientations (Fig. 5). Moreover, now the resulting spectral profile is given by a rectangular function $\Theta[(E-\omega_{if})/kv'_A]$ instead of a Lorentzian (18) (see also Fig. 5).

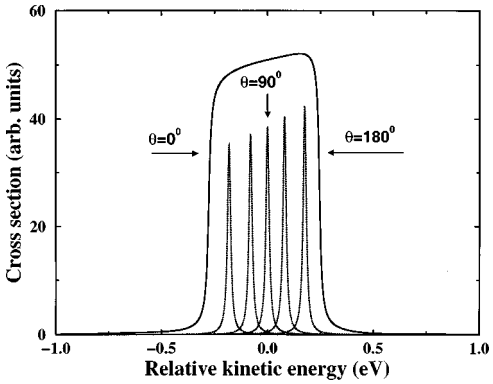

FIG. 5. Doppler broadening caused by random orientation of molecules. The ρ function (22) is shown as a solid line, while the Doppler-shifted Lorentzians [Eq. (18)] are depicted as dotted lines. Specific values $m_A=m_B$ for O_2 are used. $\Gamma=0.01$ eV, $E=500$ eV, $\Omega=2$ eV, and $\Delta=0.47$ a.u.

A. Role of the E dependency of the Doppler shift on the RXS spectral shape

As one can see from Figs. 5 and 6, the real RXS profile differs from the rectangular function $\Theta(E-\omega_{if})$ [Eq. (24)] due to the E dependency of the Doppler shift (23) (Fig. 6). This profile, shown in Fig. 6, reminds one of a trapezoid rather than a rectangle. The main reason for this distortion of the Θ function is the multiplier $1/kv'_A$ in the expressions for the ρ function [Eqs. (22) and (24)]. According to Eq. (24), the RXS cross section tends to zero when $|E-\omega_{if}|>kv'_A$. This means that outside of the Doppler band the E dependency of the Doppler shift is not so important (Fig. 6).

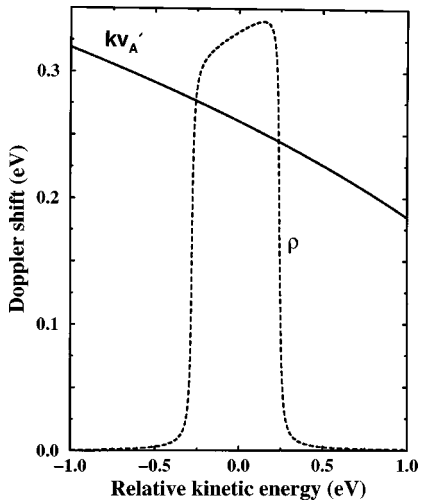

FIG. 6. The dependence of the Doppler shift kv'_A on the relative kinetic energy of the Auger electron $E-\omega_{if}$ for $\theta=0°$. Input data are the same as for Fig. 5.

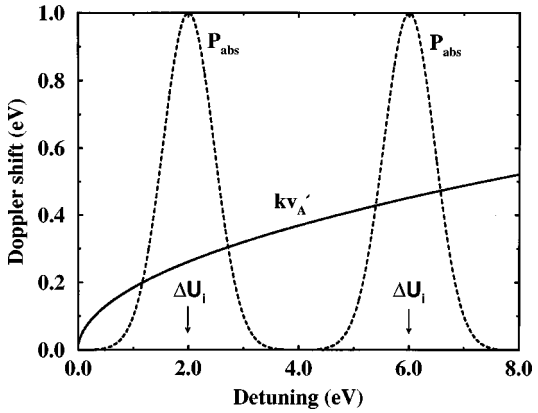

FIG. 7. The dependence of the Doppler shift kv_A' on the detuning $\Omega=\omega-\omega_{i0}$ of the incident photon frequency ω relative to the resonant frequency of the ''adiabatic transition'' ω_{i0} ($\theta=0°$). This dependence is important only when the photoabsorption probability (dashed line) $P_{\rm abs}(\Omega)\propto\langle i,\epsilon|0\rangle^{(0)2}\propto\exp[-(\Omega-\Delta U_i/\gamma_i)^2]$ is large [see Eq. (11)]. $\Delta U_i=2$ eV. $\gamma_i=0.66$ eV. Other input data are the same as for Fig. 5. The photoabsorption probability calculated for two model values of $\Delta U_i(=2$ and 6 eV) shows that the magnitude of the Doppler shift kv_A' depends strongly on the released energy ΔU_i.

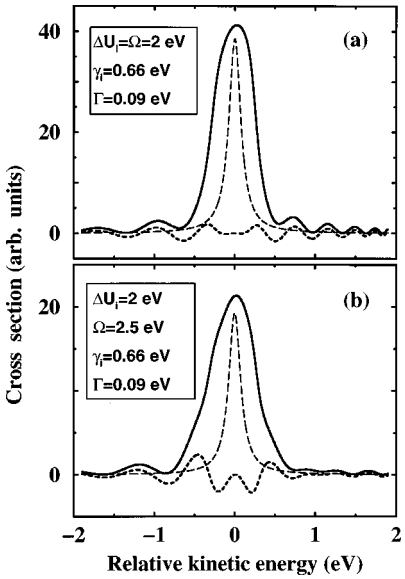

FIG. 8. The dependence of the total RXS spectral profile (solid line) $\overline{\sigma}(E,\omega)$ [Eq. (21)] on the relative kinetic energy $\nu=E-\omega_{i0}$. $E=500$ eV, $\Delta=0.47$ a.u., $E=500$ eV, and $m_A=m_B=16$. The long-dashed line shows the Lorentzian with a half-width at half-maximum (HWHM) Γ. The small second term ($\propto\chi$) (dashed line) in Eq. (21) shows interference oscillations [$\cos(2p'\Delta)$] [7].

B. Role of the ω dependency of the Doppler shift on the RXS spectral shape

Equation (23) also shows that the Doppler shift depends strongly on the excitation frequency ω. This dependency is important since it gives a possibility to actively manipulate the magnitude of the Doppler shift (see Fig. 7). It is then necessary to recall that the RXS cross section decreases strongly when the frequency ω is tuned far from the crossing point $\omega=U_i(R_0)-U_0(R_0)-\omega_0/2$ (see Fig. 7). This suppression is described by the photoabsorption bound-continuum FC factors $G(p_0)$ [Eq. (11)] with $\epsilon=\Omega$.

C. Spectral shape of the RXS atomiclike profile

Figure 8 shows results of numerical simulations of the RXS atomiclike profile [Eq. (21)], using the parameters of the potentials for O_2 [30]. The first term ($\propto\rho$) in Eq. (21) gives the main contribution to the cross section. The second smaller term at the right-hand side of this equation demonstrates oscillations [7] [$\cos(2\varphi)$], which are caused mainly by the phase difference $p'\Delta$ [see Eq. (14) of the continuum wave functions (12) for the core excited and final states]. A comparison of the total RXS profile with the Lorentzian function shows clearly the Doppler broadening of the RXS profile and its distortion due to interference of the intermediate and final continuum states.

VI. RAMAN SCATTERING BY HOMONUCLEAR DIATOMICS. ROLE OF CHANNEL INTERFERENCE

RXS by homonuclear diatomic molecules qualitatively differs from the scattering by heteronuclear ones [14]. To take into account the indistinguishability of the two atoms, one needs to sum their partial scattering amplitudes

$$F=F_1+F_2=f_1e^{-\imath qR_f}+f_2e^{\imath qR_f}, \tag{26}$$

$$q=\tfrac{1}{2}k\cos\theta,\quad R_f=\max\{x_f,x_i\},$$

where f_j is given by Eq. (17). The phases $-\imath qR_f$ and $\imath qR_f$ for different scattering channels differ only by the sign according to the expression for the radius vectors of sites for first and second atoms [Eq. (9)] in the center of gravity of the molecule. To avoid unnecessary complications, let us analyze the RXS cross section, taking into account only the main term in the scattering amplitudes (16) and (17). Contrary to intuition, the scattering amplitudes f_1 and f_2 for atoms 1 and 2 are different:

$$f_{1,2}\sim\frac{\Upsilon_{1,2}\chi_f a_{\rm n}G(p_0)e^{\imath\varphi}}{\nu\pm\mathcal{D}\cos\theta-\imath\Gamma},\quad \mathcal{D}\equiv\frac{kv'}{2},$$

$$\chi_f=\begin{cases}1 & \text{if } x_i>x_f\\ e^{-\Gamma\Delta/v_0} & \text{if } x_f>x_i.\end{cases} \tag{27}$$

Here $\mathcal{D}$ is the Doppler shift, $v_0=(2\Omega/\mu)^{1/2}$, the signs $(-)$ and $(+)$ correspond to the atoms 1 and 2, respectively, $\nu=E-\omega_{i0}$ is the detuning of the energy E of the Auger electron from the resonant frequency, and the phase φ is defined in Eq. (16). The atomic (one-center) parameter $a_{\rm n}$ is given here for atom 1. The important distinction of f_1 and f_2 has a simple physical meaning. The different signs of the Doppler shifts for atoms 1 and 2 are caused by the motion of these atoms in opposite directions ($v_1=-v_2$) in the center of gravity frame. Clearly, the absolute values of the atomic velocities are the same ($v'/2$) ($v'=p'/\mu$ is the relative velocity of the atoms).

Another important distinction between the scattering amplitudes f_1 and f_2 is their relative sign [14] given by the symmetry parameter $\Upsilon_{1,2}=\pm1$. The sign of $\Upsilon_{1,2}$ is defined by the symmetry of the electronic wave functions involved in the scattering process. Without loss of generality, let us

choose $\Upsilon_1=1$. One can easily understand that the sign of Υ_2 depends only on the parity of the product $0\otimes j$ of parities 0 and f of ground and final electronic states

$$\Upsilon_2=\begin{cases} 1 & \text{if } 0\otimes f=u, \\ -1 & \text{if } 0\otimes f=g. \end{cases} \tag{28}$$

The atomiclike resonance is formed in the dissociative region (Fig. 1) by the decay transitions to the set of final states of the same energy. Due to this degeneracy, one cannot distinguish these states in the experiment and, hence, the RXS cross section must be summed over the full degenerate manifold. However, as is well known, the x-ray scattering by identical atoms has specific spectral and anisotropic peculiarities caused by the interchannel interference [14]. According to Eqs. (27) and (28), the gerade and ungerade final states give interference contributions ($\sim f_1^* f_2$) of opposite signs. The interference terms of gerade and ungerade states can therefore suppress each other in the total cross section. (For brevity we restrict ourselves to a couple of gerade and ungerade states below—the summation over other final state quantum numbers can be done very easily.)

The quantity of interest is the cross section

$$\sigma(E,\omega)=\sigma_1+\sigma_2+\sigma_{\rm int} =\sum_{f=g,u}\left[|f_1|^2+|f_2|^2+2\,\mathrm{Re}(f_1^* f_2 e^{\imath kR_f\cos\theta})\right] \tag{29}$$

which can be measured in *electron-ion coincidence spectroscopy*. The first two terms $\sigma_{1,2}=\Sigma_f|f_{1,2}|^2$ correspond to the independent scattering channels through the core excited state in atoms 1 and 2, respectively. The interference term $\sigma_{\rm int}$ at the right-hand side describes the diffractional scattering of the Auger electron at the A_2 molecule. When this interference term is large, the two scattering channels are strongly coherent and vice versa.

Let us analyze the RXS cross section (29) for the common case of the gerade ground state

$$\sigma_{1,2}=\frac{C}{(\nu\mp\mathcal{D}\cos\theta)^2+\Gamma^2}, \qquad \sigma_{\rm int}=2C\Delta\sigma(\cos\theta), \quad \Delta\sigma(\cos\theta)=(w_u\sigma^u-w_g\sigma^g), \tag{30}$$

$$\sigma^f=\frac{[\cos(kR_f\cos\theta)\{\nu^2+\Gamma^2-(\mathcal{D}\cos\theta)^2\}+2\Gamma\mathcal{D}\cos\theta\sin(kR_f\cos\theta)]}{[(\nu-\mathcal{D}\cos\theta)^2+\Gamma^2][(\nu+\mathcal{D}\cos\theta)^2+\Gamma^2]},$$

where $C\propto|a_{\rm n}G(p_0)|^2(\chi_g^2+\chi_u^2)$. Contrary to the x-ray scattering by heteronuclear molecules [Eq. (20)], now two dissociative cones and two resonant angles exist: $\cos\theta_r=\pm 2\nu/kv'$ (in accordance with the oppositely propagated atoms).

These equations show that gerade and ungerade final states take part in the scattering process with the different weights:

$$w_f=\frac{\chi_f^2}{\chi_g^2+\chi_u^2}, \quad f=g,u. \tag{31}$$

The physical reason for this effect was given in Sec. IV [see also Eq. (27)]. A quite unusual result is here obtained: Since $w_g\neq w_u$, the interference term does not cancel after summation over gerade and ungerade final states, which in the dissociative region have the same energies.

Figure 9 shows the anomalously strong dependence of the RXS cross section on the angle θ between directions of the Auger electron and the ion propagation. The interference term leads to sharp oscillations of the cross section. A comparison of Figs. 9(a) and 9(b) demonstrates the strong dependence of the scattering anisotropy on the potential of gerade and ungerade final states through the weights w_g and w_u. As one can see from these figures, the scattering anisotropy is very sensitive also to the energy E of the Auger electron.

A. Parity selection rules

A negligibly small electron Doppler effect is the common case for x-ray spectroscopy. Therefore, it is interesting to consider the atomiclike resonance when the electron Doppler shift $\mathcal{D}$ is small in comparison with the lifetime broadening Γ. The RXS cross section being the sum of gerade and ungerade contributions then collapses in this case to the single Lorentzian

$$\sigma(E,\omega)=\sigma_g(E,\omega)+\sigma_u(E,\omega), \qquad \sigma_{g,u}(E,\omega)=2Cw_{g,u}\,\frac{1\mp\cos(kR_{g,u}\cos\theta)}{\nu^2+\Gamma^2}, \quad \mathcal{D}\ll\Gamma. \tag{32}$$

Here $-$ and $+$ correspond to gerade and ungerade ionic final states, respectively. The angular dependences of the partial cross sections $\sigma_g(E,\omega)$ and $\sigma_u(E,\omega)$ (Fig. 10) demonstrate the strong oscillations with the total suppression of gerade and ungerade contributions for angles $\theta=\theta_+$ and $\theta=\theta_-$,

$$\cos(kR_g\cos\theta_+)=1, \quad \cos(kR_u\cos\theta_-)=-1, \tag{33}$$

respectively. This remarkable decrease of the partial cross sections down to zero constitutes nothing else than a parity selection rule for Auger decay transitions.

To understand this parity selection rule let us recall that in the general case one cannot distinguish gerade and ungerade continuum wave functions of high-energy Auger electrons due to the degeneracy of these states, and the parity selection

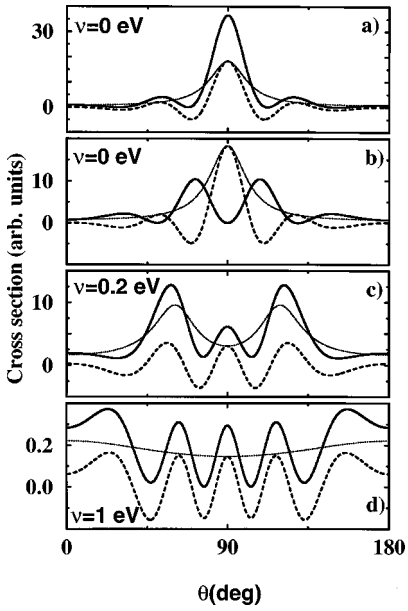

FIG. 9. The angular dependence of the total RXS profile $\overline{\sigma}(E,\omega)$ (solid line), interference contribution (dashed line) [Eqs. (29), (30), and (21)], and direct term $\sigma_1+\sigma_2$ (dotted line) for different relative kinetic energies $\nu=E-\omega_{i0}$. Input data are the same as for Fig. 11. The Doppler shift is equal to $\mathcal{D}=0.4$ eV. $\nu=E-\omega_{if}$. $w_u=1$ and $w_g=0$ everywhere, except plot (b), where $w_g=1$ and $w_u=0$. These values for the weights w_u and w_g correspond to Fig. 12.

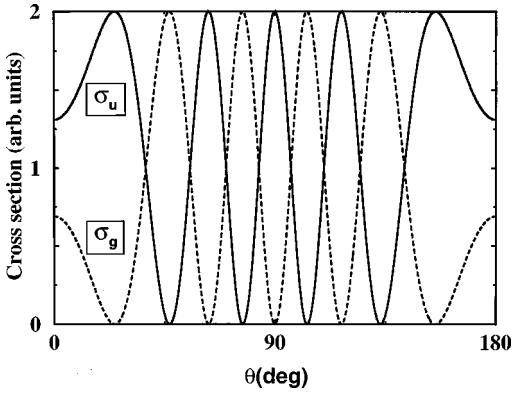

FIG. 10. The interference oscillations of the partial RXS cross sections $\sigma_g(E,\omega)$ and $\sigma_u(E,\omega)$ [Eq. (32)] for small Doppler broadening. θ is the angle between the Auger electron momentum $\mathbf{k}$ and the molecular axis. The parity selection rules take place for angles θ for which $\sigma_g(E,\omega)=0$ or $\sigma_u(E,\omega)=0$. Input data are the same as for Fig. 11.

rules are in general absent. To see this let us rewrite the Auger electron wave function $\psi_{\mathbf{k}}(\mathbf{r})$ [Eq. (5)] in the form convenient for the symmetry analysis

$$\psi_{\mathbf{k}}(\mathbf{r})=e^{i\epsilon}(\psi_{\mathbf{k1}}+e^{ikR_f\cos\theta}\psi_{\mathbf{k2}}). \tag{34}$$

Here $\mathbf{R}_f=\mathbf{R}_2-\mathbf{R}_1$, $\epsilon=\mathbf{k}\cdot\mathbf{R}_1$, and $\psi_{\mathbf{ki}}=\psi_{\mathbf{k}}(\mathbf{r}-\mathbf{R}_i)$, $\psi_{\mathbf{ki}}=0$ when $|\mathbf{r}-\mathbf{R}_i|>R_f/2$. We used the last assumption only here, and only to emphasize the locality of the Auger transition in the dissociative region. It is easy to check that the wave function (34) and this assumption yield exactly the same result [Eq. (32)].

Representation (34) shows immediately that the Auger electron wave function is odd $[\psi_{\mathbf{k}}(\mathbf{r})\sim\psi_{\mathbf{k1}}-\psi_{\mathbf{k2}}]$ and even $[\psi_{\mathbf{k}}(\mathbf{r})\sim\psi_{\mathbf{k1}}+\psi_{\mathbf{k2}}]$ under inversion through the molecular center for the angles $\theta=\theta_-$ and $\theta=\theta_+$ respectively [Eq. (33)]. The parity selection rules for the angles $\theta_\pm$ is a direct consequence of this symmetry. Indeed, the decay transition from an ungerade core excited state to a gerade final state is forbidden if the Auger electron wave function is even ($\theta=\theta_+$) and, vice versa, the ungerade-ungerade decay is not allowed when the the Auger electron wave function is odd ($\theta=\theta_-$).

We would like to stress that interference contributions $w_{g,u}\cos(kR_{g,u}\cos\theta)$ are maximal in points (33). Just as for radiative RXS [14], the symmetry selection rules can thus be considered to be a consequence of channel interference. A very similar phenomenon takes place for dissociative resonances in radiative RXS [31].

The first impression is that these parity selection rules are not observable since the total cross section (32) is the sum of gerade and ungerade contributions, and since the critical angles $\theta_\pm$ [Eq. (33)] do not coincide with each other. However the scattering to one of the final states is strongly suppressed. The reason for this is the following. Very often the final-state potential curves for gerade and ungerade states differ qualitatively from each other [10] if the classical turning point x_f for the gerade final state lies to the left of the point of the vertical photoabsorption transition $x_i\simeq R_0$ [Fig. 3(a)], then the turning point for the ungerade state is lying to the right of x_i [Fig. 3(b)] and vice versa. Equations (27) and (31) show the strong suppression of one of the final states with $x_f>x_i$ [Fig. 3(b)] due to large $\Delta=|x_f-x_i|\sim 2$ a.u. [10]. For example, $w_g\simeq 0.1$ and $w_u\simeq 0.9$ when $x_g>x_i$ and $x_u<x_i$, and vice versa if $x_g<x_i, x_g>x_i$ (other input data are the same as for Fig. 11). The angular dependence of the RXS cross section (32) for these two cases depicted in Fig. 10 shows practically total quenching of the cross section for $\cos(kR_g\cos\theta)=1$ [Fig. 10(a)].

It is easy to understand that this pure interference effect $(\sigma_{g,u}(E,\omega)\propto[1\mp\cos(kR_{g,u}\cos\theta)])$ [Eq. (32)], generating parity selection rules, is a general phenomenon and thus that it also takes place for ordinary ''molecular'' RXS transitions near the equilibrium molecular geometry, which of course poses a simpler possibility for observation. The molecular axis can also be fixed by weak adsorption on a crystalline surface [4] (see Sec. VIII). To keep the identity of atoms, the molecular axis must then lie in the surface plane. The partial cross sections $\sigma_g(E,\omega)$ and $\sigma_u(E,\omega)$ [Eq. (32)] can be measured separately, since final gerade and ungerade states have different energies.

B. Distinction of ''left'' and ''right'' atoms in A_2 molecule. Large Doppler shift

The RXS profile measured in the electron-ion coincidence spectroscopy has the following doublet structure in the Doppler limit $\mathcal{D}\gg\Gamma$ if $\theta=0°$ (or 180°)

$$\sigma(E,\omega)\simeq C\left(\frac{1}{(\nu-\mathcal{D})^2+\Gamma^2}+\frac{1}{(\nu+\mathcal{D})^2+\Gamma^2}\right)\quad\text{if } \mathcal{D}\gg\Gamma. \tag{35}$$

These two narrow Lorentzians correspond to two opposite

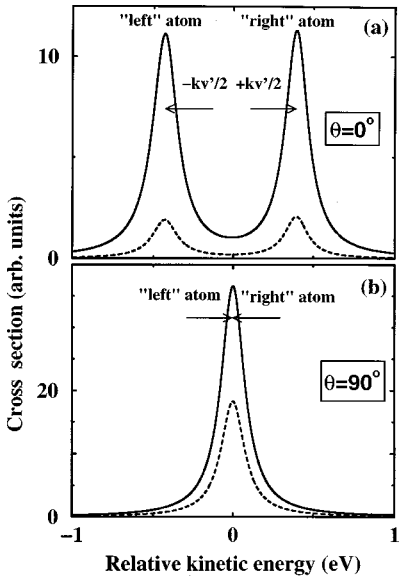

FIG. 11. The dependence of the total RXS spectral profile (solid line) $\overline{\sigma}(E,\omega)$ [Eqs. (29) and (30)] on the relative kinetic energy $\nu = E-\omega_{i0}$. $E=500$ eV, $R_c=2.28$ a.u., $\Omega=5$ eV, and $\Gamma=0.09$ eV. The interference contribution $\sigma_{\rm int}$ is depicted with the dashed line. When $\theta=0°$, the ''left'' atom has a red Doppler shift, while the ''right'' atom has a blue Doppler shift. The equivalent atoms can be distinguished by the the Doppler labels $\pm kv'/2$. One cannot distinguish these atoms when $\theta=0°$, since in this case the Doppler shift is absent.

directions of the dissociating atoms. The large Doppler shift $\mathcal{D}$ destroys the coherence of the scattering channels $\sigma_{\rm int}/\sigma(E,\omega)\sim\Gamma/kv'\ll 1$ (Fig. 11). This means that the two scattering channels now are totally independent. Moreover, one can distinguish these channels since one now can select either of them through the ''left-propagating'' and ''right-propagating'' atoms. It is possible to do so since the ''left'' and ''right'' atoms moving in opposite directions $-\mathbf{v}'/2$ and $\mathbf{v}'/2$ have different ''Doppler labels'' (Doppler shifts): $-\mathbf{k}\cdot\mathbf{v}'/2$ and $\mathbf{k}\cdot\mathbf{v}'/2$. We can say that the photon is scattered by the ''left'' (or ''right'') atom when the energy of Auger electron is equal to $E=\omega_{if}-\mathbf{k}\cdot\mathbf{v}'/2$ (or $E=\omega_{if}+\mathbf{k}\cdot\mathbf{v}'/2$). In this case only the ''left'' (or ''right'') atom is in resonance with the Auger electron, while the partial cross section for the other atom is close to zero [see Eq. (35) and Fig. 11].

When the Auger electron is emitted perpendicular to the molecular axis, the RXS profile collapses to a single Lorentzian [Eq. (32)] because $\cos\theta=0$ and the Doppler shift then is exactly equal to zero (Fig. 11). Since the Doppler shift is absent when $\theta=90°$, one cannot distinguish equivalent atoms in an A_2 molecule. In this case both scattering channels are strongly coherent and the interference term $\sigma_{\rm int}$ takes a maximal value [see Eq. (32) and Fig. 11].

The angular dependence of the total cross section and the interference contribution (Fig. 9) shows interference oscillations according to $\sin(kR_f\cos\theta)$ and $\cos(kR_f\cos\theta)$ in Eq. (30) (Fig. 9). These oscillatory features provide structure information, and can be observed when the interference parameter kR_f exceeds π.

C. Orientational averaging of cross sections for identical atoms

We now turn back to the ordinary RXS measurements in which the flux of Auger electrons is collected from all molecules. The cross section (29) must be averaged in this case over all molecular orientations. This is the procedure used in Sec. V (see also the end of Appendix B). Averaging the cross section (30) over θ, we obtain

$$\overline{\sigma}(E,\omega)=2\sigma_0 G^2(p_0)(\mathcal{X}_g^2+\mathcal{X}_u^2)(\rho+\Lambda),$$
$$\Lambda=\frac{\Gamma}{2\pi}\int_{-1}^{1}d\xi\;\Delta\sigma(\xi), \tag{36}$$

where the ρ function is given by Eq. (22) with $v_A'=v'/2$ and $\xi=\cos\theta$. Contrary to Eq. (30), the averaging procedure leads to the same partial cross sections, $\overline{\sigma_1}=\overline{\sigma_2}=2\sigma_0 G^2(p_0)\rho$. The coherence or interference term $\overline{\sigma}_{\rm int}=2\sigma_0 G^2(p_0)\Lambda$ can be much simplified (see Appendix B), since very often the diffractional parameter kR_f is large:

$$kR_f\gg 1. \tag{37}$$

For example, $kR_f\simeq 14$ for O_2. As follows directly from Eq. (B3) in Appendix B, the interference contribution (36)

$$\Lambda=\frac{\Gamma}{2\pi\mathcal{D}^2}\,(w_u\mathcal{P}_u-w_g\mathcal{P}_g), \tag{38}$$

can be approximated outside of the Doppler band as

$$\mathcal{P}_f\simeq\mathcal{P}_{f0}=2\mathcal{D}^2\,\frac{(\nu^2+\Gamma^2-\mathcal{D}^2)j_0(kR_f)+2\Gamma\mathcal{D}n_0(kR_f)}{[(\nu-\mathcal{D})^2+\Gamma^2][(\nu+\mathcal{D})^2+\Gamma^2]},$$
$$|\nu|>\mathcal{D},\quad kR_f\gg 1. \tag{39}$$

Here $j_0(x)=\sin x/x$ and $n_0(x)=-\cos x/x$ are the spherical Bessel functions of zero order. According to Eq. (B6), the interference term consists of two qualitatively different subterms

$$\mathcal{P}_f\simeq 2\pi kR_f j_0\left(kR_f\,\frac{\nu}{\mathcal{D}}\right)\exp\left(-kR_f\,\frac{\Gamma}{\mathcal{D}}\right)+\mathcal{P}_{f0},$$
$$|\nu|<\mathcal{D},\quad kR_f\gg 1, \tag{40}$$

when the Auger energy is inside the Doppler band. The direct numerical evaluation of the integral (36) shows very good agreement with the approximate formulas (39) and (40), except for small deviations near the Doppler shifts: $\pm\mathcal{D}$.

The first term at the right-hand side of Eq. (40) is caused by the pole singularities of the integrand (36) lying in the dissociation cone: $\cos\theta=\pm\nu/\mathcal{D}$ (see Appendix B). Close to resonance ($\nu=E-\omega_{if}=0$) this term, being the main contributions to $\overline{\sigma}_{\rm int}$, exceeds the second contribution ($\propto\mathcal{P}_{f0}$) by $\pi(kR_f)^2$ times. We stress that the terms (39) and (40) show the typical oscillations caused by the interference of the ejected Auger electron. However, the character of these damping oscillations is different: $j_0(kR_f)$, $n_0(kR_f)$, and $j_0(kR_f\nu/\mathcal{D})$.

The narrow line contribution to the interference term (40) demonstrates, for large $|\nu|$, a weak damping ($\sim 1/\nu$) in com-

parison with $\mathcal{P}_{f0}$ and the direct term ρ, whereas a quenching of this contribution for large Γ is much faster $[\sim\exp(-kR_f\Gamma/\mathcal{D})]$ than $\mathcal{P}_{f0}$ and ρ.

Atomiclike profiles for small Doppler broadening

When the Doppler broadening is small the atomic line profile collapses to a single Lorentzian [Eq. (36)],

$$\overline{\sigma}(E,\omega)=\overline{\sigma}_g(E,\omega)+\overline{\sigma}_u(E,\omega),$$

$$\overline{\sigma}_{g,u}(E,\omega)=\overline{\sigma}_0 w_{g,u}\,\frac{1\mp j_0(kR_{g,u})}{\nu^2+\Gamma^2}, \tag{41}$$

with $\overline{\sigma}_0=2\sigma_0 G^2(p_0)(\mathcal{X}_g^2+\mathcal{X}_u^2)\Gamma/\pi$. The second equation strongly reminds us of the structure of the radiative RXS cross section [14] if k is replaced by the change of the x-ray photon momentum under scattering and $\mp\rightarrow\pm$. Like for radiative RXS [14], the cross section (41) demonstrates the parity selection rules in the limit $kR_{g,u}\ll 1$ (see also Sec. VI A). However, contrary to radiative RXS, the transitions between the ground and final states of the same parity are forbidden in resonant Auger for $kR_{g,u}\ll 1$ due to the qualitatively different decay operators (4) and (6).

D. Supernarrowing of the atomiclike resonances

At this stage we point to the striking role of the interchannel interference in the narrowing of the RXS spectral profile up to a half-width at half maximum (HWHM) of

$$\Delta\nu\simeq\frac{\mathcal{D}}{kR},\quad R=\min\{R_g,R_u\}, \tag{42}$$

which thus does not depend on the lifetime broadening Γ. This lifetime free narrowing effect origins entirely from the single oscillating factor $j_0(kR_f\nu/\mathcal{D})$ in Eq. (40) (see also Appendix B). For example, we have for O_2 with $\Omega=0.5$ eV: $\Delta\nu\simeq 0.03$ eV ($\mathcal{D}=kv'/2\simeq 0.4$ eV, $kR\simeq 14$). Figure 12 shows that the RXS profile consists of a narrow peak or hole with the HWHM $\Delta\nu\simeq 0.03$ eV [Eq. (42)] smaller than the lifetime broadening $\Gamma=0.09$ eV [30] and a broad Doppler pedestal ($\propto\rho$) [Eq. (22)]. Let us note that we have here reached the thermal energy since $\Delta\nu\sim k_BT\sim 0.03$ eV. This means that rotational broadening must now be taken into account together with the recoil effect (see Appendix A).

Let us compare the ratio of the maximal values of the narrow-band and the direct ($\overline{\sigma}=\overline{\sigma}_1+\overline{\sigma}_2$) contributions to the cross section

$$\frac{\overline{\sigma}_{\rm nar}}{\overline{\sigma}}=2(w_u\kappa_u e^{-\kappa_u}-w_g\kappa_g e^{-\kappa_g}), \tag{43}$$

which was estimated as $\Delta\Lambda/\rho$ for $\nu=0$. Here $\Delta\Lambda$ is the first term on the right-hand side of Eq. (40). This equation shows that the relative intensity $\overline{\sigma}_{\rm nar}/\overline{\sigma}$ of the supernarrow contribution caused by the channel interference depends on the dimensionless parameter

$$\kappa_f=\frac{\Gamma}{\mathcal{D}}\,kR_f, \tag{44}$$

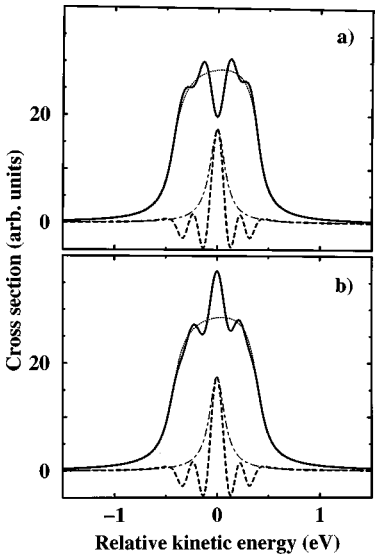

FIG. 12. The narrowing below the lifetime broadening and below the spectral width of the incident radiation. $\Delta=2$ a.u. The dependence of the total RXS profile $\overline{\sigma}(E,\omega)$ (solid line), the interference contribution (dashed line) [Eqs. (29), (30), and (21)], and the direct term ($\propto\rho$) [Eq. (22)] on the relative kinetic energy $\nu=E-\omega_{if}$. The interference term is scaled by a factor of 2. The comparison with the Lorentzian with a HWHM equal to Γ (dot-dashed line) shows the narrowing below Γ. (a) $x_u>x_i$, $x_g<x_i(w_u-w_g<0)$. (b) $x_u\langle x_i,x_g\rangle x_i(w_u-w_g>0)$. Input data are the same as for Fig. 11.

being the product of the parameter kR_f and the ratio of the lifetime broadening Γ and Doppler shift $\mathcal{D}$.

The role of the diffractional parameter (from the point of view of observation of the narrowing effect) is twofold. The width [Eq. (43)] of this resonance decreases when kR increases. However, its strength [Eq. (43)] increases only when κ_f changes from zero up to $\kappa_f=1$. The strength of the narrow resonance is quenched for $\kappa_f>1$ (Fig. 13). So a value of κ_f close to 1 gives optimal conditions for observation of this narrowing effect.

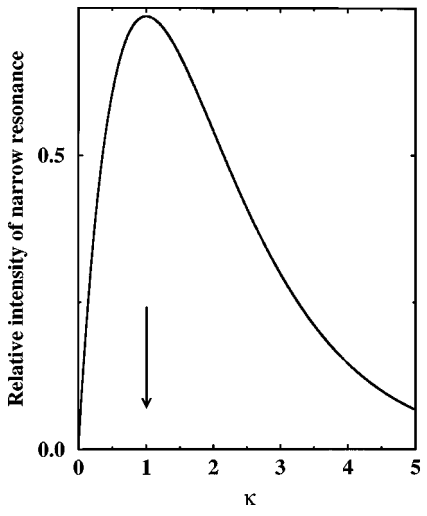

FIG. 13. The relative intensity $\overline{\sigma}_{\rm nar}/\Delta\overline{\sigma}=2\kappa\exp(-\kappa)$ [Eq. (43)] of the narrow resonance as a function of the dimensionless parameter $\kappa=\Gamma kR/\mathcal{D}$ [Eq. (44)] for the cases $w_u=1$ and $w_g=0$. Input data are the same as for Fig. 11.

1. Qualitative picture of the narrowing effect

Most of our attention in Sec. V was directed toward a formal description of the narrowing effect. As one can see from Eqs. (38) and (40), the reason for this narrowing effect is the interference or coherence term $\overline{\sigma}_{\rm int}=2\sigma_0 G^2(p_0)\Lambda$. Let us now try another way to see qualitatively the physical reason of the supernarrowing of the atomiclike resonance. The left and right atoms eject Auger electrons at different angles ($\cos\theta=\pm\nu/\mathcal{D}$, $\mathcal{D}=kv'/2$). This leads to the suppression of the interference contribution $\sigma_{\rm int}$ or coherence between scattering channels 1 and 2 if the energy of the Auger electron does not coincide with the resonant frequency: $\nu=E-\omega_{if}\neq 0$. However, both scattering channels are strongly coherent, and so the interference term takes a maximal value for the exact resonance: $\nu=0$. In this case the Auger electron is emitted perpendicular to the molecular axis, $\theta=\pi/2$. But the uncertainty relation implies that this angle $\pi/2$ is known only to within $\Delta\theta\lesssim\lambda/R$ or

$$\Delta\theta\lesssim\frac{1}{kR}, \tag{45}$$

where λ is the electron wavelength. The uncertainty in angle leads to an uncertainty $\Delta\nu$ of the Auger electron energy ν, since $\cos(\pi/2-\Delta\theta)=\Delta\nu/\mathcal{D}\simeq\Delta\theta$. Combining these two results, one obtains $\Delta\nu\lesssim\mathcal{D}/kR$, which agrees with Eq. (42).

2. Role of the spectral width of incident x-ray radiation

Up to now we have investigated the Raman scattering of monochromatic x-ray radiation. To describe a realistic experimental situation using incident radiation with a finite spectral width γ_c, we need to convolute the RXS cross section with the spectral function of incoming photons $\Phi(\omega-\omega_c,\gamma_c)$ centered at frequency ω_c. The x-ray Raman scattering through the continuum intermediate states qualitatively differs from the case of discrete intermediate states. Contrary to the latter case, the cross section (2) does not contain the δ function when the final state for the atomiclike resonance is a continuum state. This means that the RXS cross section can be factorized: $\sigma(E,\omega)=\sigma_{\rm abs}(\omega)I(E,v')$. Here we select the atomic photoabsorption cross section $\sigma_{\rm abs}(\omega)\sim\sigma_0 G^2(p_0)$ and the rest part $I(E,v')$ of the cross section which depends on the energy of the Auger electron E and on the incident photon frequency via the relative nuclear velocity in final continuum state $v'=[2(\omega-\omega_{i0}-\nu)/\mu]^{1/2}$. Let us remind the reader that the position ($E=\omega_{if}$) of the atomiclike resonance does not depend on the excitation energy [8,7,9]. One can expect only some small changes of the width and spectral shape of this resonance due to v'. Consider here the typical experimental situation when the spectral width γ_c does not exceed a few eV (for example, $\gamma_c\lesssim 5$ eV). The photoabsorption FC factor $G(p_0)$ [Eq. (11)] drops out fast when ω is tuned from the vertical photoabsorption frequency ω_{i0}^s [Eq. (7)] at a distance larger than the width γ_i of $G(p_0)$. This means that the photoabsorption FC factor ''cuts off'' the width $\gamma_i\lesssim 1$ eV from the spectral band of the incident photon flux. One can show that the changes of the atomiclike profile can be neglected when ω is changed in this narrow region close to the vertical photoabsorption transition. For example, a change $\delta\omega\sim\gamma_i\sim 1$ of eV leads to the following relative change of the width $\Delta\nu$ [Eq. (42)]: $\delta\Delta\nu/\Delta\nu\sim\gamma_i/2\Omega\sim 1\%$. This means that with good accuracy the RXS cross section convoluted with the spectral function can be factorized as

$$\langle\overline{\sigma}(E,\omega_c)\rangle=\int\Phi(\omega-\omega_c,\gamma_c)\overline{\sigma}(E,\omega)d\omega \simeq I(E,v_0)\langle\sigma_{\rm abs}(\omega_c)\rangle. \tag{46}$$

Here we obtained one of the important features of the atomiclike resonance: The narrowing up to $\Delta\nu$ [Eq. (42)] practically does not depend on the spectral width of the incident radiation. The main reason for this is that the position of the supernarrow atomiclike resonance ($\nu=E-\omega_{if}=0$) [Eq. (40)] does not depend on the frequency of incident radiation [8,7,9]. Equation (46) also allows us to conclude that the shape of the atomiclike resonance in practice does not depend on the spectral width γ_c.

VII. POSSIBILITY FOR EXPERIMENTAL OBSERVATION

A few words about the possibility for experimental observation of the Doppler effects are in order. We can foresee three important points concerning the choice of the molecular system. The main requirement is to excite above the dissociation threshold so as to obtain a release energy of $\Delta U_i>1$ eV (see Fig. 1). For example, the first core excited state $^3\Pi_u$ of O_2 with $\Delta U_i\lesssim -1$ eV [30] does not satisfy this condition. Of course, one can tune ω above the vertical resonant frequency $\omega_{i0}^s=U_i(R_0)-U_0(R_0)-\omega_0/2$. But this is possible only if ω does not exceed ω_{i0}^s by the width of the photoabsorption FC factor [Eq. (11)] $\gamma_i\sim 1$ eV. The core excitation to higher energies leads to an exponential quenching of the RXS cross section.

The effects discussed for the homonuclear diatomics can also be observed for other symmetrical molecules. The recent photoelectron-energy-selected photoion coincidence experiment with BF_3 [32] showed a release energy of more than 4 eV for the F^+ ions. The corresponding electron Doppler shift is approximately equal to 0.55 eV, which is larger than the lifetime broadening ($\Gamma\sim 0.1$ eV) of the $|1s_F^{-1}\rangle$ state. So one can expect that the BF_3 molecule is a good candidate for observation of both Doppler broadening and supernarrowing. However, in the BF_3 case the manifestation of the diffractional scattering and narrowing effect can be complicated due to the Jahn-Teller effect caused by vibronic coupling of degenerate core excited states.

The fact that the electron Doppler shift must be larger than the lifetime broadening makes it preferable to measure light atoms or homonuclear molecules. The intensity of the supernarrow peak or hole (Fig. 12) strongly depends on the distance between the classical turning points $|x_g-x_u|$ [Eq. (43)] for the gerade and ungerade final states. For example this intensity is equal to zero when $x_g=x_u$. However, the analysis of the potential curves for the different final (''optically excited'') states shows [10] that in many cases $|x_g-x_u|$ is large, and has the order of magnitude 1 Å.

VIII. SUMMARY

We have presented a theory for Doppler effects in resonant radiative and nonradiative x-ray scattering. The treat-

ment of the excitation and the subsequent decay of the dissociative core excited state as a single quantum-mechanical process, also accounting for the site-dependent phase factors, reveals moderately large electron Doppler effects for the nonradiative RXS resonances. There are two main reasons behind this: the large momentum **k** of the Auger electron, and the large kinetic-energy and hence atomic velocity release following dissociation. A strong resonance correlation between the directions of the ion and electron yields exists, since the Doppler shift depends on the angle between the molecular axis and the Auger electron momentum. This strong anisotropy should be measurable in electron-ion coincidence spectroscopy. The RXS atomiclike profile for molecules with chaotical orientations is broadened due to the angular dependence of the Doppler effect.

It is difficult to expect an importance of the Doppler effect for radiative RXS due to the small value of the photon momentum $k_{\rm ph}$. For example, $k_{\rm ph}\simeq 0.14$ a.u., while the electron momentum is $k\simeq 6$ a.u. for O_2. Of course, the Doppler broadening increases with the atomic number, but the lifetime broadening increases as well, and only if these dependences ''cross'' each other can one expect a photon Doppler effect for atomiclike resonances.

As is well known, systems with symmetry-related atoms are very specific for x-ray Raman scattering owing to the interference of the scattering channels through core excited states localized at the different identical atoms [12–19]. The present investigation gives yet another example of this fact, showing that the dissociative resonances in RXS by homonuclear molecules are associated with interesting spectral and anisotropical features.

We have stressed the principal possibility to distinguish identical atoms with opposite propagation in dissociative states. This is because they have opposite Doppler shifts and hence different resonant frequencies. The corresponding measurements can be realized via the electron-ion coincidence technique. Even without a Doppler effect, interference plays a very important role in the angular-resolved electron-ion coincidence measurements. We found strong interference oscillations of the cross section versus the angle between propagation directions of the Auger electron and the fragment of dissociation.

Among other results predicted in this work, we would like to stress the parity selection rules in the resonant Auger effect, and that this is a general phenomenon also valid for the RXS transitions, like bound-bound transitions close to the equilibrium molecular geometry. The physical reason for this is found in the interference of the Auger electrons and the exact parity of the wave function of Auger electrons for critical angles between the molecular axis and the Auger electron momentum. It is easy to understand that this purely interference effect is not caused by the Doppler effect and molecular dissociation, and thus that this phenomenon should be observable both for atomiclike resonances by means of electron-ion coincidence measurements and for the ordinary bound-to-bound RXS transitions close to the equilibrium geometry of the molecule. In the latter case the molecular axis can be fixed with the help of (weak) adsorption on a crystalline surface. The qualitatively different angular dependencies (oscillations with opposite phases) of cross sections for gerade and ungerade states thus constitutes a tool for symmetry assignments in Auger and electron coincidence spectroscopies.

Another prediction presented in this work is a supernarrow peak or hole on top of a Doppler pedestal, having a measurable width which goes below not only the lifetime broadening but also the spectral width of the incident radiation. The existence of these peculiarities is based on the rather unexpected result that final gerade and ungerade states give contributions to the RXS cross section with different weights, which implies that the interference term does not cancel. The formal reason for this can be found in the difference of the potential surfaces, and hence the distinction of the classical turning points for the gerade and ungerade final states. These features, caused by the channel interference, have unusual spectral profiles given by the spherical Bessel function of zero order. The oscillatory spectral shape shows directly the interference origin of the narrowing mechanism. The estimations show that the width of the supernarrow features is comparable with the thermal energy $k_BT\simeq 0.03$ eV. This means that the rotational broadening and recoil effect can also be important for setting the final width of these resonant features.

ACKNOWLEDGMENTS

This work was supported by the Swedish National Research council (NFR). We wish to thank Dr. V. Carravetta and Dr. T. Privalov for a critical reading of the manuscript and for fruitful discussions.

APPENDIX A: ROLE OF ROTATIONAL DEGREES OF FREEDOM

Due to thermal motion, the ground-state rotational levels are populated according to Boltzmann statistics,

$$(2J+1)\exp\left(-\frac{BJ(J+1)}{k_BT}\right), \tag{A1}$$

where k_B is the Boltzmann constant, $B=1/2I$ and J are the rotational constant and the rotational quantum number with $I=1/\mu R_0^2$ as the moment of inertia. This distribution is at a maximum near

$$J_{\rm max}=\frac{k_BT}{2B}. \tag{A2}$$

Let us estimate $J_{\rm max}$ for O_2 with $B\simeq 1.6\times 10^{-4}$ eV. $J_{\rm max}\simeq 28\gg 1$ at room temperatures ($k_BT\simeq 0.03$ eV). Thus the classical description of the rotational degrees of freedom is applicable due to large values of J and small spacing $[2B(J+1)\simeq 2BJ_{\rm max}\simeq 0.009$ eV] between adjacent rotational levels in comparison with the lifetime broadening $\Gamma\simeq 0.09$ eV.

The rotational structure in RXS can be broadened due to the excitation and deexcitation spectral transitions. The photoabsorption cannot essentially broaden the rotational band since only $J\rightarrow\pm 1,0$ rotational transitions are allowed in photoabsorption.

According to Eq. (13), the strength of the rotational transitions under Auger decay is governed by the following matrix element between the rotational states $|jm\rangle$ of a diatomic molecule:

$$\langle jm|e^{-\imath\alpha kx\cos\theta}|j_1m_1\rangle. \tag{A3}$$

Due to such an exponential dependence of the integrand on the rotational angle θ, one cannot say in advance how strong the change of J will be under the decay transition. It is also difficult to say something certain about selection rules when $\alpha kx>1$. However, for large values of J, the classical treatment of the molecular rotation is applicable, and one can then estimate the broadening of the rotational band ΔE_J of the Auger decay.

For the ground state the rotational energy of a molecule with the angular momentum $L_0=I_0\omega_{\rm rot}^0$ is equal to $E_{\rm rot}^0=L_0^2/2I_0$, where $\omega_{\rm rot}^0$ and $I_0=\mu R_0^2$ are the angular velocity and moment of inertia, respectively. The angular momentum is not changed if the incident radiation is linearly polarized. This means that the angular momentum is the same, $L=I\omega_{\rm rot}=L_0$, if the molecule dissociates on the core excited potential surface up to internuclear distance x. Now the rotational energy $E_{\rm rot}=L^2/2I$, moment of inertia $I=\mu x^2$, and angular velocity are different. Let us assume that atom A in the point x emits the Auger electron with the speed u at the angle θ with respect to the molecular axis. The angular momentum conservation law allows us to find the angular momentum of the molecule L_f after emission of the Auger electron: $L_f=L-xu_\perp$, $u_\perp=u\sin\theta$. After the ejection of the Auger electron the rotational energy of the molecule $E_{\rm rot}^f=L_f^2/2I=E_{\rm rot}+\delta E_{\rm rot}$ is changed by the value

$$\delta E_{\rm rot}=-m_eu_0u_\perp\frac{R_0}{x}+\frac{m_eu_\perp^2}{2\mu}, \tag{A4}$$

where $u_0=\sqrt{2E_{\rm rot}^0/\mu}\simeq\sqrt{2k_BT/\mu}$. One can say also that this change is caused by the recoil effect. We write this equation in ordinary units (not a.u.) to see explicitly the role of the ratio m_e/μ. The estimation for O_2 with the Auger electron energy $m_eu^2/2=500$ eV shows that $|m_eu_0u_\perp R_0/x|<0.06R_0/x$ eV ($R_0/x<1$) and $m_e^2u_\perp^2/2\mu\simeq0.03$ eV. So the emission of the Auger electron leads to an additional broadening of the RXS spectral profile. However, we neglect this broadening, since $|\delta E_{\rm rot}|<0.06$ eV is smaller than the lifetime broadening $\Gamma=0.09$ eV. Moreover, $|\delta E_{\rm rot}|$ is essentially smaller than the Doppler broadening of the RXS profile discussed in Sec. V. The rotational mechanism of the broadening of the RXS spectral lines can though be important in RXS spectroscopy with superhigh resolution at higher temperatures.

APPENDIX B: ASYMPTOTIC FORM OF THE INTERFERENCE TERM

As shown in Sec. VI C, the diffractional parameter kR_f is very often large [Eq. (37)]. To evaluate the integral (36), it is useful to start directly from the definition of the interference term (29) and the partial amplitude of scattering [Eq. (27)]

$$\overline{\sigma}_{\rm int}=\sigma_0G^2(p_0)\,\frac{2\Gamma}{\pi\mathcal{D}^2}\,(\mathcal{X}_g^2+\mathcal{X}_u^2)(w_u\mathcal{P}_u-w_g\mathcal{P}_g),$$

$$\mathcal{P}_f=-\,{\rm Re}\int_{-1}^{1}d\xi e^{\imath kR_f\xi_\phi(\xi)}, \tag{B1}$$

with $\xi=\cos\theta$. This integral has three singularities. The first one refers to the strong oscillations due the large parameter kR_f [Eq. (37)], while the next two refer to the poles of the integrand,

$$\phi(\xi)=\frac{1}{(\xi-\widetilde{\nu}-\imath\Gamma)(\xi+\widetilde{\nu}-\imath\widetilde{\Gamma})}, \tag{B2}$$

lying in the upper half-plane. Here we introduced the dimensionless Auger detuning $\widetilde{\nu}=\nu/\mathcal{D}$ and lifetime broadening $\widetilde{\Gamma}=\Gamma/\mathcal{D}$ to see directly the asymptotical calculation of this integral.

When the energy of the Auger electron is outside the Doppler band $|\widetilde{\nu}|>1$, the integrand (B2) has no singularities on the real axis ξ. The existence of the large parameter (37) resulting from the strong oscillation of the integrand considerably simplifies the evaluation of integral (B1). Integrating by parts, we obtain

$$\mathcal{P}_f=\mathcal{P}_{f0}+0\left(\frac{1}{(kR_f)^2}\right),$$

$$\mathcal{P}_{f0}=-\,{\rm Re}\,\frac{1}{\imath kR_f}\,[e^{\imath kR_f}\phi(1)-e^{-\imath kR_f}\phi(-1)],\quad |\nu|>\mathcal{D}. \tag{B3}$$

With the energy of the Auger electron inside the Doppler band $|\widetilde{\nu}|<1$, integrand (B2) has two resonant features $\xi=\pm\widetilde{\nu}$ on the real axis ξ. It is convenient to partition the integral (B1) into three regions:

$$\mathcal{P}_f=-\,{\rm Re}\left\{\int_{-\infty}^{\infty}-\int_{1}^{\infty}-\int_{-\infty}^{-1}\right\}d\xi\;e^{\imath kR_f\xi}\phi(\xi). \tag{B4}$$

The first integral is obtained exactly by the residue theorem, while the last two integrals can be evaluated the same way as integral (B3), since the integrand has no features in the region $|\xi|\geqslant1$ outside the dissociative cone: $\cos\theta=\pm\nu/\mathcal{D}$. This integral thus leads to the supernarrow resonance: If the expression for the ϕ function [Eq. (B2)] is rewritten as

$$\phi(\xi)\equiv\frac{1}{2\widetilde{\nu}}\left(\frac{1}{\xi-\widetilde{\nu}-\imath\widetilde{\Gamma}}-\frac{1}{\xi+\widetilde{\nu}-\imath\widetilde{\Gamma}}\right), \tag{B5}$$

one can see that the lifetime broadening is canceled in the resonant denominator $\widetilde{\nu}$. This results in

$$\mathcal{P}_f\simeq\frac{2\pi}{\widetilde{\nu}}\sin(kR_f\widetilde{\nu})e^{-kR_f\widetilde{\Gamma}}+\mathcal{P}_{f0},\quad |\nu|<\mathcal{D},\quad kR_f\gg1. \tag{B6}$$

One then obtains the remarkable result that the interference contribution (B1) to the cross section contains a term with the lifetime free resonant factor

$$\frac{1}{\nu}=\frac{1}{E-\omega_{if}}, \tag{B7}$$

which is exactly the first multiplier on the right-hand side of the expression for the ϕ function, Eq. (B5).

The molecular orientation is hidden in the atomic photoabsorption and decay operators (factor $|a_{\mathbf{n}}|^2$). As one can see directly from Eq. (B3), the shortwave asymptote (37) corresponds to a molecular orientation along $\mathbf{k}$ ($\xi=\cos\theta=\pm1$). Thus $|a_{\mathbf{n}}|^2$ may be extracted from the integral with $\mathbf{n}\|\mathbf{k}$. Close to the resonance with the dominating supernarrow term (B6), $\mathbf{k}$ is orthogonal to the molecular axis since $\cos\theta=\pm\nu/\mathcal{D}\simeq0$. In that case, the factor $|a_{\mathbf{n}}|^2$ can be extracted from the integral with $\mathbf{n}\perp\mathbf{k}$.

[1] J. Nordgren, J. Electron Spectrosc. Relat. Phenom. **78**, 25 (1996).

[2] T. Åberg and B. Crasemann, in *Resonant Anomalous X-Ray Scattering. Theory and Applications*, edited by G. Materlik, C. J. Sparks, and K. Fischer (North-Holland, Amsterdam, 1994), p. 431.

[3] P. L. Cowan, in *Resonant Anomalous X-Ray Scattering. Theory and Applications* (Ref. [2]), p. 449.

[4] N. Mårtensson, in *Applications of Synchrotron Radiation*, edited by W. Eberhardt, Springer Series in Surface Sciences Vol. 35 (Springer-Verlag, Berlin, 1995), p. 65.

[5] W. Eberhardt, in *Applications of Synchrotron Radiation* (Ref. [4]), p. 203.

[6] P. P. Kane, Radiat. Phys. Chem. **50**, 31 (1997).

[7] F. Gel'mukhanov and H. Ågren, Phys. Rev. A **54**, 379 (1996).

[8] E. Kukk, H. Aksela, S. Aksela, F. Gel'mukhanov, H. Ågren, and S. Svensson, Phys. Rev. Lett. **76**, 3100 (1996).

[9] O. Björneholm, S. Sundin, S. Svensson, R. R. T. Marinho, A. Naves de Brito, F. Gel'mukhanov, and H. Ågren, Phys. Rev. Lett. **79**, 3150 (1997).

[10] J. I. Steinfeld, *Molecules and Radiation. An Introduction to Modern Molecular Spectroscopy* (Harper & Row, New York, 1974).

[11] J. H. Eland and E. Duerr (unpublished).

[12] F. Gel'mukhanov, L. N. Mazalov, and N. A. Shklyaeva, Zh. Eksp. Teor. Fiz. **69**, 1971 (1975) [Sov. Phys. JETP **42**, 1001 (1975)].

[13] F. Gel'mukhanov, L. N. Mazalov, and N. A. Shklyaeva, Zh. Eksp. Teor. Fiz. **71** 960 (1976) [Sov. Phys. JETP **44**, 504 (1977)].

[14] F. Gel'mukhanov and H. Ågren, Phys. Rev. A **49**, 4378 (1994).

[15] Y. Ma, K. E. Miyano, P. L. Cowan, Y. Aglizkiy, and B. A. Karlin, Phys. Rev. Lett. **74**, 478 (1995).

[16] F. Gel'mukhanov and H. Ågren, J. Phys. B **29**, 2751 (1996).

[17] P. Glans, K. Gunnelin, P. Skytt, J.-H. Guo, N. Wassdahl, J. Nordgren, H. Ågren, F. Gel'mukhanov, T. Warwick, and E. Rotenberg, Phys. Rev. Lett. **76**, 2448 (1996).

[18] P. Glans, P. Skytt, K. Gunnelin, J.-H. Guo, and J. Nordgren, J. Electron Spectrosc. Relat. Phenom. **82**, 193 (1996).

[19] F. Gel'mukhanov and H. Ågren, Phys. Rev. B **57**, 3780 (1998).

[20] D. Turner, C. Baker, A. Baker, and C. Brundle, *Molecular Photoelectron Spectroscopy* (Wiley, New York, 1970).

[21] V. Carravetta, F. Kh. Gel'mukhanov, H. Ågren, S. Sundin, S. J. Osborne, A. Kikas, O. Björneholm, A. Ausmees, and S. Svensson, Phys. Rev. A **56**, 4665 (1997).

[22] J. J. Sakurai, *Advanced Quantum Mechanics* (Addison-Wesley, Reading, MA, 1991).

[23] F. Gel'mukhanov and L. N. Mazalov, Opt. Spectrosk. **42**, 659 (1977) [Opt. Spectrosc. **42**, 371 (1977)].

[24] F. Gel'mukhanov, T. Privalov, and H. Ågren, Phys. Rev. A **56**, 256 (1997).

[25] S. Sundin, F. Gel'mukhanov, H. Ågren, S. J. Osborne, A. Kikas, O. Björneholm, A. Ausmees, and S. Svensson, Phys. Rev. Lett. **79**, 1451 (1997).

[26] A. Cesar, F. Gel'mukhanov, Y. Luo, H. Ågren, P. Skytt, P. Glans, J.-H. Guo, K. Gunnelin, and J. Nordgren, J. Chem. Phys. **106**, 3439 (1997).

[27] A. V. Golovin, N. A. Cherepkov, and V. V. Kuznetsov, Z. Phys. D **24**, 371 (1992).

[28] E. Shigemasa, J. Adachi, M. Oura, and A. Yagishita, Phys. Rev. Lett. **74**, 359 (1995).

[29] F. Heiser, O. Geßner, U. Hergenhahn, J. Viefhaus, K. Wieliczek, N. Saito, and U. Becker, J. Electron Spectrosc. Relat. Phenom. **79**, 415 (1996).

[30] M. Neeb, J.-E. Rubensson, W. Biermann, W. Eberhardt, K. J. Randall, J. Feldhaus, A. L. D. Kilcoyne, A. M. Bradshaw, Z. Xu, P. D. Johnsson, and Y. Ma, Chem. Phys. Lett. **212**, 205 (1993).

[31] F. Gel'mukhanov, T. Privalov, and H. Ågren (unpublished).

[32] Y. Shimizu, K. Ueda, H. Chiba, M. Okunishi, K. Ohmori, J. B. West, Y. Sato, and T. Hayaishi, J. Chem. Phys. **107**, 2419 (1997).